An Impedance Investigation of the Mechanism of Pure Magnesium Corrosion in Sodium Sulfate Solutions

Geneviève Baril, Gonzalo Galicia, Claude Deslouis, Nadine Pébère, Bernard Tribollet, Vincent Vivier

An Impedance Investigation of the Mechanism of Pure Magnesium Corrosion in Sodium Sulfate Solutions

Geneviève Baril,[a] Gonzalo Galicia,[b] Claude Deslouis,[b,*] Nadine Pébère,[a,*,z] Bernard Tribollet,[b,*] and Vincent Vivier[b,*]

[a]*Centre Inter Universitaire de Recherche et d'Ingénierie des Matériaux, UMR CNRS 5085, ENSIACET, 31077 Toulouse Cedex 04 France*
[b]*UPR 15 du CNRS, LISE, Université Pierre et Marie Curie, 75252 Paris, France*

The corrosion behavior of pure magnesium in sodium sulfate solutions was investigated using voltammetry and electrochemical impedance spectroscopy with a rotating disk electrode. The analysis of impedance data obtained at the corrosion potential was consistent with the hypothesis that Mg corrosion is controlled by the presence of a very thin oxide film, probably MgO, and that the dissolution occurs at film-free spots only. This hypothesis was substantiated both by the superposition of the EIS diagrams, obtained for different immersion times and for two Na_2SO_4 concentrations once normalized, and by use of scanning electrochemical microscopy in the ac mode to sense the local conductivity of the material. On the basis of the electrochemical results, a model was proposed to describe magnesium corrosion at the open-circuit potential. Simulation of the impedance diagrams was in good agreement with the experimental results.

[DOI: 10.1149/1.2401056]

Magnesium is an attractive metal because of its low density and its relative abundance in seawater. Magnesium alloys offer a high potential for use as a lightweight structural material in such transport applications as automobiles and aircraft.[1] However, due to the high reactivity of magnesium, its corrosion resistance is low, which limits applications. In a recent study, the corrosion behavior of as-cast magnesium alloys (AM50 and AZ91) was investigated in a sodium sulfate solution by electrochemical impedance spectroscopy (EIS).[2] At the corrosion potential and for short immersion times (<6 h), the impedance diagrams presented the same phenomenology as that obtained for pure magnesium (three time constants with the same characteristic frequencies).[3,4] Thus, for short exposures to the aggressive solution, in spite of the presence of coarse intermetallic particles (Mg–Al and Mg–Al–Mn) in the matrix of the alloys and of eutectic areas in grain boundaries of AZ91 alloy, the corrosion behavior of the alloys was close to that of pure magnesium. This was explained by the fact that at the beginning of immersion, the coarse intermetallic particles and the eutectic areas remained unaffected due to galvanic coupling between these zones and the grain body. Thus, for short immersion times, the impedance diagrams represent the corrosion process of the grain body because both the coarse particles and the eutectic areas are cathodic and therefore protected against corrosion. Song et al.[5] have already pointed out that the α matrix phase in AZ magnesium alloys follows the same corrosion mechanisms as pure magnesium. Thus, a better understanding of the corrosion mechanisms of pure magnesium is a prerequisite for a comprehensive approach of the mechanisms involved in magnesium alloy corrosion. In fact, although numerous studies have been devoted to pure magnesium, the corrosion mechanism remains unclear.

The anodic dissolution of magnesium is accompanied by an anomalous phenomenon called the negative difference effect (NDE). It is characterized experimentally by an unexpected increase of the cathodic hydrogen evolution reaction when the anodic overvoltage is increased. To explain the magnesium corrosion and more particularly this NDE phenomenon, several mechanisms have been proposed including the formation of magnesium hydrides,[6] metastable monovalent ions,[7-12] and magnesium hydroxides and oxides.[13-23] Song et al.[11,12] recently proposed a new mechanism for the NDE. They explained that the formation of a partially protective layer of $Mg(OH)_2$ plays an important role in the corrosion behavior of magnesium. They considered the following reactions in their discussion of the NDE

$$2H^+ + 2e^- \rightarrow H_2 \quad \text{(cathodic partial reaction)} \qquad [1]$$

$$2Mg \rightarrow 2Mg^+ + 2e^- \quad \text{(anodic partial reaction)} \qquad [2]$$

$$2Mg^+ + 2H_2O \rightarrow 2Mg^{2+} + 2\,OH^- + H_2 \quad \text{(chemical reaction NDE)} \qquad [3]$$

$$2Mg + 2H^+ + 2H_2O \rightarrow 2Mg^{2+} + 2\,OH^- + 2H_2 \quad \text{(overall reaction)} \qquad [4]$$

$$Mg^{2+} + 2\,OH^- \rightarrow Mg(OH)_2 \quad \text{(corrosion product formation)} \qquad [5]$$

The dissolution mechanism is based on an increase in the film-free areas with increasing anodic potential on which the anodic and cathodic partial reactions (Eq. 1 and 2) can occur more easily than on the surface covered by a film. In the film-free areas, these authors assumed that magnesium corrosion occurs with the production of univalent ions. For high anodic overpotentials, the rate of the chemical reaction is increased due to the increased concentration of Mg^+ produced by Reaction 2 and concomitantly, there is an increase in the amount of hydrogen evolved. Song et al.[11,12] mentioned that the protective film is potential dependent in that there is complete film coverage over the whole surface and a low rate of corrosion for potentials below the pitting potential. According to these authors, the pitting potential is slightly more negative than the corrosion potential. In the proposed mechanism, the electrochemical production of divalent magnesium ions was never considered. In addition, the mechanisms of formation and dissolution of the protective film are not taken into account in the corrosion process.

The aim of the present work is to report experimental data obtained in sodium sulfate solutions in view of modeling magnesium corrosion. DC and transient electrochemical measurements were complemented by local electrochemical measurements [scanning electrochemical microscopy (SECM)] to obtain a more complete understanding of the behavior of magnesium in neutral media. On the basis of the experimental results and data taken from the literature, a new model for describing Mg corrosion at the open-circuit potential is presented.

Experimental

Material.— The corrosive medium was a sodium sulfate proanalysis grade solution (pH 5.6). Two Na_2SO_4 concentrations were tested, 0.01 and 0.1 M. In a previous paper,[4] it was shown that the presence of O_2 does not influence the corrosion of magnesium. In fact, magnesium corrosion is relatively insensitive to the oxygen

* Electrochemical Society Active Member.
z E-mail: Nadine.Pebere@ensiacet.fr

concentration because water reduction is the main cathodic reaction involved in the corrosion process. The authors concluded, however, that the protective properties of the film formed on the magnesium surface were dependent on the aeration of the electrolyte due to the presence of CO_2. They postulated that HCO_3^- increased the rate of dissolution of the corrosion product layer by formation of soluble salts. In the present work, the volume of solution used was 200 mL and the electrolyte was in contact with air. The temperature was maintained at 25°C. The HCO_3^- concentration determined previously under these conditions was about 40 mg L^{-1}.[4] The working electrode was a rotating disk of 1 cm^2 surface area consisting of the cross section of a cylindrical magnesium rod, provided by Alfa Company. The purity was 99.95%. The body of the rod was covered with a heat-shrinkable sheath, leaving only the cross section of the cylinder in contact with the solution. Prior to any experiment, the electrode was polished with SiC paper down to grade 4000, cleaned in water in an ultrasonic bath, and then dried in warm air. The counter electrode was a platinum grid. A saturated K_2SO_4/Hg_2SO_4 electrode (SSE) was used as a reference.

Electrochemical measurements.— The polarization curves were plotted under potentiostatic regulation using a Solartron 1286 Electrochemical Interface. They were plotted (point by point) by steps of 20 mV every 2 min to ensure quasi-steady-state conditions. The anodic and cathodic parts were obtained independently starting from the corrosion potential. The ohmic drop in the electrolyte was dependent on the sodium sulfate concentration. As a consequence, the polarization curves were corrected from the ohmic drop experimentally determined from electrochemical impedance measurements. The correction on the imposed potential was 80% of the ohmic drop measured at the corrosion potential to avoid instability. Electrochemical impedance measurements were carried out using a Solartron 1250 frequency response analyzer in a frequency range of 65 kHz to a few mHz with eight points per decade. The linearity of the system was checked by varying the amplitude of the ac signal applied to the sample.

SECM.— The SECM apparatus used in this study was a homemade device already described elsewhere.[24,25] It consisted of a 3-axis positioning system (VP-25XA, Newport) driven by a motion encoder (ESP300, Newport) allowing a spatial resolution of 100 nm in the three directions. The electrochemical measurements were carried out with a homemade bipotentiostat coupled to a low-noise current-to-voltage converter (Femto DLPCA200, FBI Optilas) with an adjustable gain (10^3–10^{11} V/A) and a large bandwidth (up to 500 kHz). In order to evaluate the electrolyte resistance (R_e), the high-frequency (HF) impedance measurement was coupled to the SECM, and the impedance modulus of the electrode tip was measured with an homemade analog device.[24] A sinusoidal voltage (frequency f_{HF} of 75–150 kHz and peak-to-peak amplitude $V_{p\text{-}p}$ of 10–50 mV) delivered by a function generator (TG550, TTi) was superimposed on the dc voltage of the potentiostat. The output analog signal was sent to the R_e-measurement channel that delivered a voltage signal $V_{Re}(t)$, which was proportional to the amplitude of the ac current and, therefore, was a linear function of the reciprocal of the impedance modulus $Mod(Z_{HF})$ at the frequency f_{HF}, according to the relationship

$$V_{Re} = \frac{b_1}{Mod(Z_{HF})} + b_2$$

This technique, based on impedance-modulus measurements, has been shown to give exact values of R_e inasmuch as calibration curves obtained with pure resistors were used to evaluate the constants b_1 and b_2. The R_e variations were then interpreted as local variations of the surface reactivity with a spatial resolution depending on both the electrode dimension and the tip-to-substrate distance. In our case, the spatial resolution was in the micrometer range.

Moreover, it was demonstrated that the electrolyte resistance was dependent on the tip-to-interface distance and also on the nature of the interface;[24,26] R_e increased when the ultramicroelectrode (UME) approached an insulator, whereas it decreased for a conductor. Therefore, it is possible to detect local changes in reactivity or conductivity at the interface by measuring the electrolyte resistance.[26,27]

SECM tips consisted of homemade platinum microelectrodes. The 5 μm radius platinum wire was sealed into soft glass. The normalized radius of the UME $RG = r_g/a$ (where a and r_g are the radii of the platinum wire and the tip-insulating material, respectively) was set between 10 and 20 and was determined by both scanning electron microscope observation and by recording an approach curve at an insulating substrate.[28]

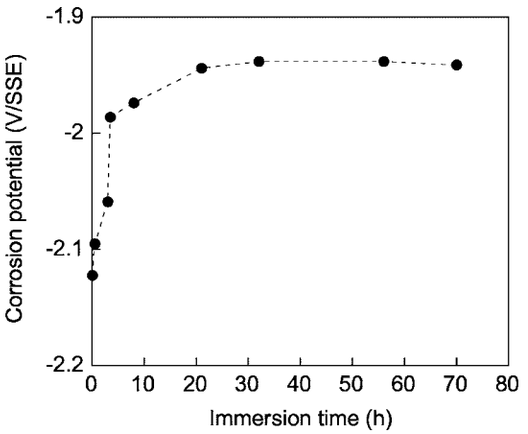

Figure 1. Corrosion potential of pure magnesium as a function of time in a 0.1 M Na_2SO_4 solution; electrode rotation rate: 240 rpm.

Results and Discussion

DC measurements.— Figure 1 illustrates the variation of the free corrosion potential, E_{corr}, of pure magnesium dipped into 0.1 M Na_2SO_4 solution. During the first 20 h of immersion, E_{corr} increases with time and then it stabilizes at approximately 32 h. This change in corrosion potential was accompanied by an increase of the pH of the medium to a value higher than 10 at the end of the experiment. This pH variation is in agreement with the global reaction of the corrosion process (Reaction 4). The shift of the corrosion potential in the anodic direction could be linked to an improvement of the protective properties of the film formed on the magnesium surface. In spite of the strong reactivity of magnesium, the time required to reach the stationary state is relatively long.

The polarization curves obtained after two preliminary hold times at the corrosion potential, E_{corr}, are reported in Fig. 2. Independent of the immersion time, the anodic part of the curves can be split into three domains: (*i*) The first domain starting from E_{corr} (low anodic overpotential) shows linear increase of the current density with the potential in Tafel coordinates. The calculated slope was lower for 32 h of immersion ($\approx$85 mV dec^{-1}) than for 3 h 30 min ($\approx$106 mV dec^{-1}). The current density decreased as the hold time at E_{corr} increased. (*ii*) The second domain is marked by an abrupt increase in the current density around −1.85 V/SSE. This potential value was independent of the immersion time and can be attributed to the change of the dominant dissolution reaction from Reaction 2 to one that involves direct formation of Mg^{2+}.[29] (*iii*) For larger potential values (>−1.85 V/SSE), a current plateau, whose height was independent of the immersion time, characterizes the third domain. The current reached 10 mA cm^{-2}. Observations after anodic polarization showed that the electrode surface was covered by a thick film of white crystals, which were identified as $Mg(OH)_2$ by X-ray diffraction.[30]

In the cathodic range, the current densities were slightly lower after 32 h of immersion at the corrosion potential than after 3 h

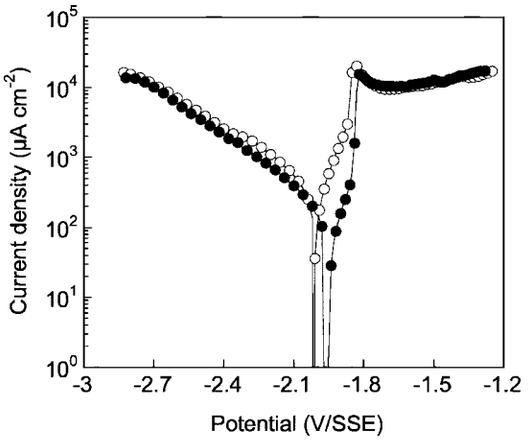

Figure 2. Current–voltage curves plotted after two preliminary hold times at the corrosion potential in a 0.1 M Na_2SO_4 solution: (○) 3 h 30 min and (●) 32 h; electrode rotation rate: 1000 rpm.

30 min. It can be considered that the cathodic branch displays a linear behavior with the semilog coordinates. The slope is particularly high around 300 mV dec^{-1}. The origin of the steepness of the slope can be attributed to hydrogen release which modifies the electrode surface. As a matter of fact, numerous bubbles were formed on the magnesium surface during cathodic sweeps. Thus, the influence of the immersion time on the polarization curves results in both a decrease of the current density in a large domain around the corrosion potential and a shift of the corrosion potential towards higher values.

When the electrode rotation rate was varied, the cathodic curves were superimposable. Thus, the cathodic process is not controlled by diffusion in the liquid phase. For the anodic part, in the second domain and on the plateau, the curves are independent of the electrode rotation rate. The anodic curves were only poorly dependent on the electrode rotation rate in the first domain starting from E_{corr} (about 100–150 mV near E_{corr}). Thus, the mechanism of pure magnesium corrosion in sulfate solutions is not controlled by the diffusion in solution. The effect of the electrode rotation rate was in good agreement with previous results.[4]

Electrochemical impedance and SECM measurements.— Figure 3a shows the impedance diagrams obtained for different hold times at E_{corr} in 0.1 M Na_2SO_4. All these diagrams are characterized by two well-defined capacitive loops, at high and medium frequencies, followed by an inductive loop in the lower frequency domain. The increase in immersion time at E_{corr} led to a size increase in both high- and medium-frequency capacitive loops and also in the inductive loop. After 32 h of immersion, a stationary state was reached, and no significant variation of the EIS response was observed. In Fig. 3b, the EIS spectra plotted in Fig. 3a are normalized by dividing the real and the imaginary parts of the diagram by the maximum value of the impedance for each diagram. It can be seen that all the diagrams can be merged into a single diagram.

Figure 4a presents the impedance diagrams obtained for two Na_2SO_4 concentrations. The shape of the diagrams was independent of the Na_2SO_4 concentration. The increase of the Na_2SO_4 concentration led to a decrease of the size of the three loops observed on the impedance diagrams. In this case again, when the impedance is normalized, the diagrams are merged into a single spectrum. Moreover, similar behavior has already been observed for the AZ91 magnesium alloy in a Na_2SO_4 solution for different values of the pH;[31] the diagrams presented the same shape and were reduced to a single diagram following the same procedure.

The merging of the diagrams (Fig. 3b and 4b) indicates that the corrosion mechanism is independent of the immersion time and the

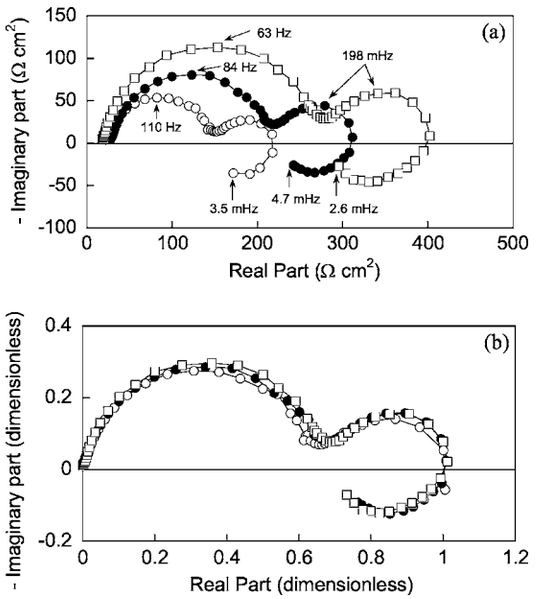

Figure 3. (a) Electrochemical impedance diagrams plotted after different hold times at E_{corr} in a 0.1 M Na_2SO_4 solution and with an electrode rotation rate of 240 rpm: (○) 1 h 30 min, (●) 21 h, and (□) 32 h. (b) Normalized impedance diagrams.

concentration of the medium. Thus, the merging of the diagrams can be explained by a change of the bare parts of the surface. In agreement with the mechanism proposed by Song et al.,[11,12] Mg corrosion is proposed to occur only in the film-free areas, and MgO is proposed to act as a protective film.

To verify this hypothesis, SECM experiments were performed using electrolyte resistance as an electrochemical sensor to visualize cracks and holes above the Mg surface after 4 and 24 h of immersion in 0.5 M Na_2SO_4 solution (Fig. 5). As the oxide layer thickness is in the nanometer range, the use of a 5 μm radius microelectrode

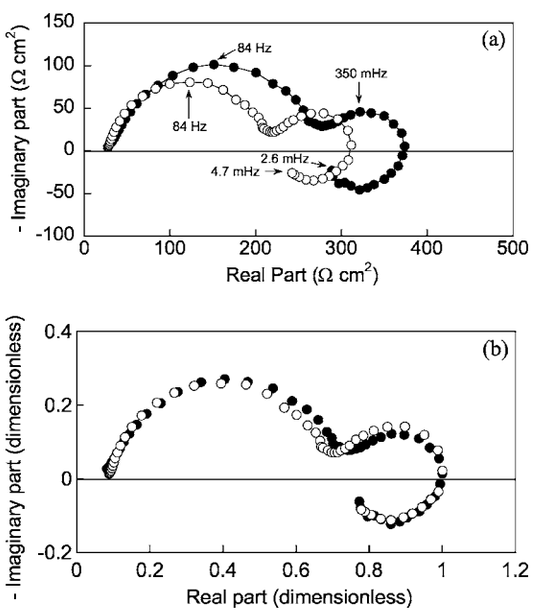

Figure 4. (a) Electrochemical impedance diagrams plotted for two Na_2SO_4 concentrations and an electrode rotation rate of 240 rpm: (○) 0.1 M and (●) 0.01 M. (b) Normalized impedance diagrams.

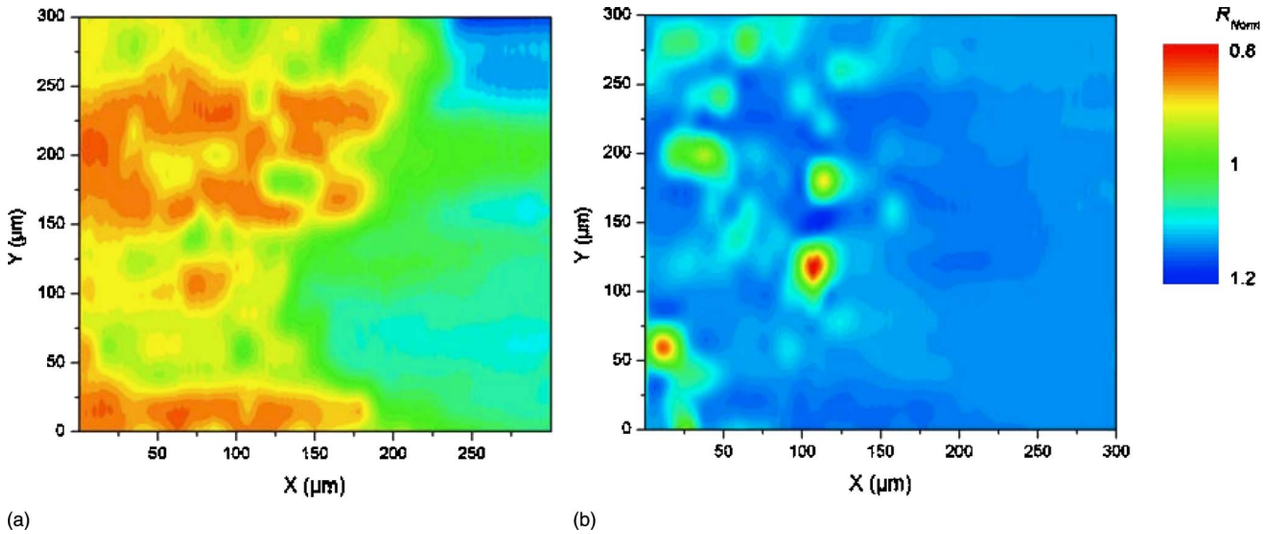

Figure 5. (Color online) Electrolyte resistance images performed using a 10 μm diameter Pt tip over Mg surface after (a) 4 and (b) 24 h of immersion in a 0.5 Na_2SO_4 solution, at 120 kHz and with 30 mV peak-to-peak amplitude. The tip velocity was 10 μm/s.

tip to scan the surface implies immunity to the surface topography, and the electrolyte resistance variations should be interpreted as variations of the local electronic conductivity of the surface only. Moreover, the ac impedance images were plotted using the dimensionless R_{Norm} quantity, that is, the ratio R_e/R_∞, where R_∞ is the electrolyte resistance far from the substrate. Figure 5a reveals that after 4 h of immersion, the Mg surface is already inhomogeneous, and thus, the oxide film has already begun to be formed, partially covering the Mg surface. Then, progressively, the insulating (MgO) layer covers larger areas of the metal surface. Figure 5b corresponds to the SECM measurement performed after 24 h of immersion over the same surface area. The influence of this MgO layer is clearly seen, and the small spots correspond to domains on which the electrolyte resistance is lower than R_∞. These domains thus correspond to the active sites for Mg dissolution. These two images are in full agreement with the hypothesis of surface variations of the active domains with time to describe Mg dissolution. However, from these data, it is difficult to extract the exact values of surface variations because the area scanned (300×300 μm) only accounts for a small portion of the immersed sample.

The MgO layer is formed progressively. The formation of MgO corresponds to the following equilibrium

$$MgO + H_2O \leftrightarrows Mg(OH)_2 \quad [6]$$

The thick and porous layer of $Mg(OH)_2$ is formed following Eq. 5. This layer is homogeneous and covers the entire Mg surface.[4] Thus, it can be assumed that active zones are moving on the magnesium surface. In other words, active zones become passive, and new active zones are created near the passive ones. Even if the presence of active zones corresponds to localized corrosion, it is not highly localized corrosion, such as pitting corrosion for aluminum and aluminum alloys, where the pit initiation is followed by a propagation step. Here, the corrosion must be interpreted in terms of a more uniform type of corrosion as evidenced by the presence of the thick porous corrosion products layer. This layer impedes the visualization of both the presence of the very thin layer of MgO and the active areas.

Schematic representation of the interface and equivalent circuit.— The electrochemical results obtained for pure magnesium in Na_2SO_4 solutions revealed behaviors which seem contradictory with its high reactivity: (*i*) the stationary state is only obtained after several hours of immersion and (*ii*) the impedance measurements could be made to very low frequencies (few mHz) without any dispersion. These impedance diagrams have been shown to be consistent with the Kramers–Kronig relations.[32] In addition, when the immersion time increased, E_{corr} was shifted in the anodic direction, the current density around E_{corr} decreased, and the impedance values increased. These results can only be explained by the presence of a protective film on the Mg surface which controls the corrosion process and whose protective properties increase with time.

On the basis of the experimental results and literature data, a schematic representation of the interface is presented in Fig. 6. Two different layers are present on the Mg surface, a thin barrier film of MgO in contact with the metal and a relatively thick porous film of $Mg(OH)_2$ on top of the barrier film. The $Mg(OH)_2$ layer coats the MgO film and the film-free areas. The Mg dissolution occurs in the film-free areas and the Mg^{2+} ions produced at the interface diffuse through the porous $Mg(OH)_2$ layer. The corresponding elements of the equivalent electrical circuit are the faradaic impedance (Z_f) in parallel with the double-layer capacitance (C_d). The MgO layer is characterized by a film capacitance (C_f) in parallel with a film resistance (R_f). The MgO oxide film is assumed to be very protective, and thus R_f is very high with respect to Z_f. Therefore, R_f has no influence on the impedance measurements and is represented as a dashed line in Fig. 6. The film-free areas are small in comparison with the surface covered by MgO (Fig. 5) and then C_d is negligible with respect to C_f. This C_f value can be extracted from the high-frequency loop, which is analyzed by considering a constant phase element (CPE) in parallel with a resistance. The origin of this CPE was recently explained using local electrochemical impedance spectroscopy and attributed to the distribution of the resistance associated with the geometry of the disk electrode (2D distribution).[33] The corresponding capacitance was deduced from Brug's formula.[34] In-

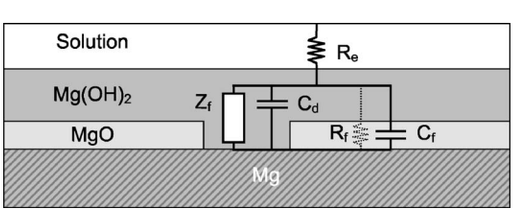

Figure 6. Schematic representation of the interface and of the equivalent circuit.

dependent of both the exposure time and of the sodium sulfate concentration, the capacitance has the same value of around 10 $\mu F/cm^2$. From the capacitance value, the thickness of the protective layer (d) can be evaluated from the relationship $d = \varepsilon\varepsilon_0 S/C$, where S is the surface area ($S = 1\ cm^2$), ε_0 the vacuum permittivity ($\varepsilon_0 = 8.85\ 10^{-14}$ F/cm), and ε the relative dielectric constant of magnesium oxide ($\varepsilon = 10$).[35] The calculated value is very low, about 1 nm. This low thickness and the presence of $Mg(OH)_2$ may explain why the MgO oxide layer was not often observed by surface analyses and was not taken into account to describe the Mg corrosion processes.[11,12]

The change of the impedance with immersion time or Na_2SO_4 concentration is due to a variation of free surface area which can explain both the observation that all impedance diagrams are identical after normalization (Fig. 3b and 4b) and also that the polarization curves are not significantly modified by the hold time at E_{corr} (Fig. 2).

Kinetics model.— The appearance of the medium-frequency capacitive loop suggests diffusion impedance. The impedance diagrams were identical when the electrode rotation rate was changed (not reported), and thus this loop can be attributed to diffusion through the porous layer of $Mg(OH)_2$. The presence of an inductive loop was independent of immersion time and of Na_2SO_4 concentration. The impedance spectra of magnesium always presented an inductive loop at low frequencies.[12,36,37] The inductive loop is present at the beginning of immersion when the thick film is not present on the Mg surface. Inductive loops are generally ascribed to the existence of relaxation processes of adsorbed species.[38,39]

A model is proposed which takes into account the different processes discussed above. In the frequency range corresponding to the impedance measurements, the film-free areas are considered to be constant for each measurement. The presence of the inductive loop in the low-frequency range involves an adsorbed species, and, as Mg^{2+} ion production occurs in two steps, Mg^+ is assumed to be the absorbed intermediate. Mg^+ is the simpler species which can be involved in the Mg corrosion as an intermediate. The mass-transport loop in the medium-frequency range corresponds to the diffusion of Mg^{2+} through the porous $Mg(OH)_2$ layer; therefore, Mg^{2+} reacts at the interface.

On the film-free areas, the two reactions considered were

$$Mg \xrightarrow{k_1} Mg^+_{ads} + e^- \qquad [7]$$

and

$$Mg^+_{ads} \underset{k_{22}}{\overset{k_2}{\rightleftharpoons}} Mg^{2+} + e^- \qquad [8]$$

To take into account the NDE, a chemical reaction similar to reaction 3 was also introduced

$$Mg^+_{ads} + H_2O \xrightarrow{k_3} Mg^{2+} + OH^- + \frac{1}{2}H_2 \qquad [9]$$

The high-frequency capacitive loop corresponds to the charge-transfer resistance of Reactions 7 and 8, in parallel to the MgO film capacitance. The charge-transfer resistance involves cathodic and anodic reactions. This kinetic model corresponds to the free areas and, in agreement with experimental observations (Fig. 4), does not involve the nature of the electrolyte.

On the basis of this reaction model, ac-impedance diagrams were calculated and simulated by assuming that the adsorbate Mg^+_{ads} obeys Langmuir's isotherm and that the rate constant of electrochemical reactions are exponentially potential dependent (Tafel's law). Each reaction (index i) has a normalized rate constant K_i corresponding to its rate constant k_i by

$$K_i = k_i \exp[b_i(E - E^0)] \qquad [10]$$

where b_i is the activation coefficient with the potential, and E^0 is an origin potential (arbitrarily chosen). Moreover, the chemical step 9 is supposed to be potential independent. Assuming that the maximum number of sites per surface unit which can be occupied by the adsorbate Mg^+_{ads} is β, the mass and charge balances are expressed as functions of the fraction of the surface coverage, θ, by the adsorbed species by

$$\beta\frac{d\theta}{dt} = K_1(1-\theta) - K_2\beta\theta + K_{22}C^{(0)}_{Mg^{2+}} - k_3\beta\theta \qquad [11]$$

$$\frac{DC^{(0)}_{Mg^{2+}}}{\delta} = K_2\beta\theta - K_{22}C^{(0)}_{Mg^{2+}} + k_3\beta\theta \qquad [12]$$

and

$$I_F = FA[K_1(1-\theta) + K_2\beta\theta - K_{22}C^{(0)}_{Mg^{2+}}] \qquad [13]$$

where F is Faraday's constant, A is the free electrode surface area, δ is the thickness of the $Mg(OH)_2$ layer, and I_F is the faradic current. $C^{(0)}_{Mg^{2+}}$ is the concentration of the Mg^{2+} ion at the electrode interface and D is the diffusion coefficient of Mg^{2+} (in the film). Mg^{2+} diffusion is supposed to occur only in the $Mg(OH)_2$ layer, which is in agreement with the fact that experimental data are independent of the electrode rotation rate. At the steady state, θ and $C^{(0)}_{Mg^{2+}}$ are thus given by

$$\theta = \frac{K_1\left(\frac{D}{\delta} + K_{22}\right)}{K_1\left(\frac{D}{\delta} + K_{22}\right) + (K_2 + k_3)\frac{D}{\delta}\beta} \qquad [14]$$

and

$$C^{(0)}_{Mg^{2+}} = \frac{\beta\theta(K_2 + k_3)}{\frac{D}{\delta} + K_{22}} \qquad [15]$$

respectively.

The faradic impedance Z_F is thus calculated by linearizing the mathematical expressions 11-13 for small sine wave perturbations, i.e.

$$[\beta j\omega + K_1 + \beta(K_2 + k_3)]\Delta\theta = [(1-\theta)K_1b_1 - \beta\theta K_2b_2 - C^{(0)}_{Mg^{2+}}K_{22}b_{22}]\Delta V + K_{22}\Delta C^{(0)}_{Mg^{2+}} \qquad [16]$$

and

$$\frac{\Delta I_F}{AF} = (K_2\beta - K_1)\Delta\theta + [(1-\theta)K_1b_1 + \beta\theta K_2b_2 + C^{(0)}_{Mg^{2+}}K_{22}b_{22}]\Delta V - K_{22}\Delta C^{(0)}_{Mg^{2+}} \qquad [17]$$

Because the specie Mg^{2+} diffuses towards the electrode surface, the resulting concentration perturbation $\Delta C^{(0)}_{Mg^{2+}}$ is obtained from the usual Warburg impedance, $N(\omega)$, with a diffusion layer of finite thickness. The resulting impedance can be expressed as

$$Z_F = \frac{\Delta V}{\Delta I_F} = \frac{\left(1 + K_{22}N(\omega)\left\{1 - \frac{(K_2\beta - K_1)}{[\beta j\omega + K_1 + \beta(K_2 + k_3)]}\right\}\right)}{AF\left\{\frac{(r_1 - r_2)(K_2\beta - K_1)}{[\beta j\omega + K_1 + \beta(K_2 + k_3)]} + (r_1 + r_2)\right\}} \qquad [18]$$

with $r_1 = (1-\theta)K_1b_1$ and $r_2 = K_2b_2\beta\theta + K_{22}b_{22}C^{(0)}_{Mg^{2+}}$

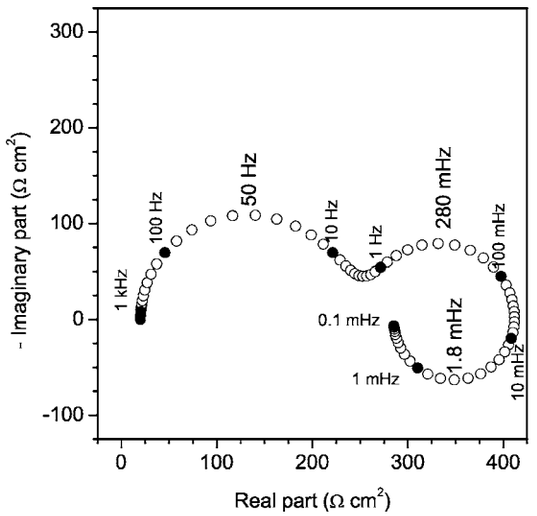

Figure 7. Simulated impedance diagram for the following parameters: $b_1 = 20\ V^{-1}$, $b_2 = 10\ V^{-1}$, $b_{22} = 10\ V^{-1}$, $k_1 = 10^{-9}\ cm^{-2}\ s^{-1}$, $k_2 = 1.5 \times 10^{-2}\ cm^{-2}\ s^{-1}$, $k_{22} = 1.5 \times 10^{-3}\ cm^{-2}\ s^{-1}$, $k_3 = 5 \times 10^{-4}\ cm^{-2}\ s^{-1}$, $\delta = 20\ \mu m$, $D = 3 \times 10^{-6}\ cm^{-2}\ s^{-1}$, $C_{dl} = 20\ \mu F\ cm^{-2}$, and $\beta = 1.5 \times 10^{-3}\ mol\ cm^{-2}$.

Finally, the overall impedance Z involves the contribution of Z_F and of the capacitance C_d and C_f (Fig. 6) reduced to C_f (see before)

$$Z = R_e + \frac{Z_F}{1 + j\omega Z_F C_f} \qquad [19]$$

where R_e is the electrolyte resistance.

An example of a simulated diagram is given in Fig. 7. It is characterized by the three loops previously described. The time-constant characteristic of each semicircle and the magnitude of the overall diagram are fully consistent with experimental data. However, these three loops are defined by six variables and the kinetics model involved at least eleven parameters, thus only six relations between the kinetics parameters can be obtained by a fitting procedure. For this reason, this study was only limited to an impedance simulation. Nevertheless, Eq. 18 can be represented as

$$Z_F = R_t\left[1 + K_{22}N(\omega) - \frac{2Sr_1K_{22}N(\omega) + (r_1 - r_2)S}{(r_1 - r_2)S + (r_1 + r_2)}\right] \qquad [20]$$

with

$$S = \frac{(K_2\beta - K_1)}{\beta j\omega + K_1 + \beta(K_2 + k_3)} \text{ and } R_t = \frac{1}{r_1 + r_2}$$

This impedance can thus be expressed as a sum of three terms

$$Z_F = R_t + R_tK_{22}N(\omega) - \frac{R_t[2r_1K_{22}N(\omega) + (r_1 - r_2)](K_2\beta - K_1)}{(r_1 + r_2)\beta j\omega + K_1 + \beta(K_2 + k_3) + (r_1 - r_2)(K_2\beta - K_1)} \qquad [21]$$

The latter expression clearly demonstrates the contribution of the charge-transfer resistance, the diffusion loop, and the inductive loop.

It should also be mentioned that the value taken by the surface coverage, θ, remains low at the corrosion potential and was estimated to have a value as low as 0.5% by the previous numerical calculations.

Conclusion

The corrosion of pure magnesium in sodium sulfate solutions was studied by voltammetry, EIS, and SECM techniques. On the basis of our experimental results and taking into account literature data, the following points have been established.

1. Magnesium corrosion is controlled by the presence of a very thin MgO oxide film, and dissolution occurs only at the bare parts of this film. Both the MgO and the film-free areas are covered by a thick porous layer of $Mg(OH)_2$.

2. The invariance of the EIS diagrams, once normalized by the maximum value of the real part, leads to the conclusion that the corrosion mechanism is independent of the electrolyte concentration and of the immersion time. It can be described as the exchange of two electrons in two successive electrochemical steps where the adsorption of the intermediate $(Mg^+)_{ads}$ is followed by two parallel paths; one is chemical and gives rise to the NDE and the other is electrochemical leading to Mg^{2+}.

3. The calculation of the impedance diagram from the proposed corrosion mechanism was shown to be in good agreement with experimental data.

Centre National de la Recherche Scientifique assisted in meeting the publication costs of this article.

References

1. G. Song and A. Atrens, *Adv. Eng. Mater.*, **5**, 837 (2003).
2. G. Baril, C. Blanc, and N. Pébère, *J. Electrochem. Soc.*, **148**, B489 (2001).
3. N. Pébère, C. Riera, and F. Dabosi, *Electrochim. Acta*, **35**, 555 (1990).
4. G. Baril and N. Pébère, *Corros. Sci.*, **43**, 471 (2001).
5. G. Song, A. Atrens, X. Wu, and B. Zhang, *Corros. Sci.*, **40**, 1769 (1998).
6. G. G. Perrault, *J. Electroanal. Chem. Interfacial Electrochem.*, **51**, 107 (1974).
7. J. W. Turrentine, *J. Phys. Chem.*, **12**, 448 (1908).
8. J. H. Greenblatt, *J. Electrochem. Soc.*, **103**, 539 (1956).
9. J. H. Greenblatt, *Corrosion (Houston)*, **4**, 125 (1962).
10. R. L. Petty, A. W. Davidson, and J. Kleinberg, *J. Am. Chem. Soc.*, **76**, 363 (1954).
11. G. Song, A. Atrens, D. Stjohn, J. Nairn, and Y. Li, *Corros. Sci.*, **39**, 855 (1997).
12. G. Song, A. Atrens, D. Stjohn, X. Wu, and J. Nairn, *Corros. Sci.*, **39**, 1981 (1997).
13. G. R. Hoey and M. Cohen, *J. Electrochem. Soc.*, **106**, 776 (1959).
14. J. L. Robinson and P. F. King, *J. Electrochem. Soc.*, **108**, 36 (1961).
15. P. F. King, *J. Electrochem. Soc.*, **110**, 1113 (1963).
16. P. F. King, *J. Electrochem. Soc.*, **113**, 536 (1966).
17. R. Tunold, H. Holtan, M. B. H. Lasson, and R. Steen-Hansen, *Corros. Sci.*, **17**, 353 (1977).
18. K. G. Cowan and J. A. Harrison, *Electrochim. Acta*, **24**, 301 (1979).
19. K. G. Cowan and J. A. Harrison, *Electrochim. Acta*, **25**, 899 (1980).
20. E. Gulbransen, *Electrochim. Acta*, **37**, 1403 (1992).
21. E. Gulbransen, J. Tafto, and A. Olsen, *Corros. Sci.*, **34**, 1423 (1993).
22. P. M. Bradford, B. Case, G. Dearnaley, J. F. Turner, and I. S. Woolsey, *Corros. Sci.*, **16**, 747 (1976).
23. D. A. Vermilya and C. F. Kirk, *J. Electrochem. Soc.*, **116**, 1487 (1969).
24. C. Gabrielli, F. Huet, M. Keddam, P. Rousseau, and V. Vivier, *J. Phys. Chem. B*, **108**, 11620 (2004).
25. C. Gabrielli, F. Huet, M. Keddam, P. Rousseau, and V. Vivier, *Electrochem. Solid-State Lett.*, **6**, E23 (2003).
26. C. Gabrielli, E. Ostermann, H. Perrot, V. Vivier, L. Beitone, and C. Mace, *Electrochem. Commun.*, **7**, 962 (2005).
27. E. N. Ervin, H. S. White, and L. A. Baker, *Anal. Chem.*, **77**, 5564 (2005).
28. J. Kwak and A. J. Bard, *Anal. Chem.*, **61**, 1221 (1989).
29. M. G. Lopez-Buisan, *Corrosion (Houston)*, **57**, 712 (2001).
30. G. Baril and N. Pébère, in *Proceedings of the International Symposium on Environmental Degradation of Materials and Corrosion Control in Metals*, M. Elboujdaini and E. Ghali, Editors, p. 55 (1999).
31. G. Baril, C. Deslouis, G. Galicia, N. Pébère, and B. Tribollet, in *Proceedings of the EUROCORR Symposium*, CDRom, paper no. O-230-F, p. 1–10 (2005).
32. M. E. Orazem, N. Pébère, and B. Tribollet, *J. Electrochem. Soc.*, **153**, B129 (2006).
33. J.-B. Jorcin, M. Orazem, N. Pébère, and B. Tribollet, *Electrochim. Acta*, **51**, 1473 (2006).
34. G. J. Brug, A. L. G. Van Den Eeden, M. Sluyters-Rehbach, and J. H. Sluyters, *J. Electroanal. Chem. Interfacial Electrochem.*, **176**, 275 (1984).
35. N. Damak, A. Kallel, and Z. Fakhfakh, *Ann. Chim. Sci. Mat.*, **23**, 255 (1998).
36. H. Zidoune, M.-H. Grosjean, L. Roué, J. Huot, and R. Schultz, *Corros. Sci.*, **46**, 3041 (2004).
37. D. Battochi, A. M. Simoes, D. E. Tallman, and G. P. Bierwagen, *Corros. Sci.*, **48**, 2226 (2006).
38. I. Epelboin, C. Gabrielli, M. Keddam, and H. Takenouti, *Electrochim. Acta*, **20**, 913 (1975).
39. I. Aoki, M.-C. Bernard, I. Cordoba de Torresi, C. Deslouis, H. G. de Melo, S. Joiret, and B. Tribollet, *Electrochim. Acta*, **46**, 1871 (2001).